Interaction Between the ENSO and the Asian Monsoon in a Coral Record of Tropical Climate

C. D. Charles, D. E. Hunter, Richard G. Fairbanks

The oxygen isotopic composition of a banded coral from the western equatorial Indian Ocean provides a 150-year-long history of the relation between the El Niño–Southern Oscillation (ENSO) phenomenon and the Asian monsoon. Interannual cycles in the coral time series were found to correlate with Pacific coral and instrumental climate records, suggesting a consistent linkage across ocean basins, despite the changing frequency and amplitude of the ENSO. However, decadal variability that is characteristic of the monsoon system also dominates the coral record, which implies important interactions between tropical and midlatitude climate variability. One prominent manifestation of this interaction is the strong amplitude modulation of the quasi-biennial cycle.

Compilations of sea surface temperature (SST) anomalies demonstrate that the ENSO phenomenon is equally important in both the Indian and Pacific oceans, which implies a climate connection over much of Earth (*1*). However, the different basinal geometry and the seasonally reversing monsoon currents demand a separate set of physical processes governing interannual temperature variability in the Indian Ocean (*2*), and, therefore, the degree of coupling between the ocean basins—a central issue for predictability—is not necessarily fixed. In fact, the tendency for this coupling to evolve may explain why the relation between the ENSO and the Asian monsoon has been the subject of one of the longest standing debates in climatology (*3*).

Previous analyses have variously concluded either that the Asian monsoon affects the ENSO or that the converse is true (*4*). Each of these conclusions allows the possibility for different large-scale feedbacks [for example, the former view implies that Eurasian snow cover could influence tropical climate (*5*)]. Yet, resolution of these dynamical effects with the instrumental record alone is compromised by the fact that continuous reliable observations rarely span more than three decades—a period arguably already modified by human activities. Thus, it is difficult to predict whether the relations determined from modern observations would apply in basic climate states different from those of recent years. Furthermore, the long records that do exist (for example, the India Monsoon Rainfall Index) may not be the most appropriate measures of the large-scale Asian monsoon phenomenon (*3*). Defining the interaction between the ENSO and the Asian monsoon requires not only an extended record but also a globally relevant index.

C. D. Charles and D. E. Hunter, Scripps Institution of Oceanography, La Jolla, CA 92093–0220, USA.
R. G. Fairbanks, Lamont Doherty Earth Observatory, Palisades, NY 10964, USA.

Here we present a 150-year record of SST from the Seychelles (southwestern equatorial Indian Ocean), which was deduced from oxygen isotope analysis in an annually banded coral. We chose this site because it represents an open ocean region, where the climate variability has shown high correlations with canonical ENSO indices (Fig. 1). We built on the principle that the interannual surface temperature changes in the western tropical Indian Ocean reflect a response (through upwelling and evaporation) to the organized atmospheric convection to the east (*6*), composed seasonally of the Asian monsoon, the Indonesian Low, and the Australian monsoon (*7*). Therefore, given the potential for both the zonal (ENSO) and monsoonal influences, the western tropical Indian Ocean surface temperature represents, in principle, an effective gauge of fundamental interactions in the global climate system. The instrumental observations from the region (*8*) were discontinuous (Fig. 1A), but the Seychelles coral record provides a long uninterrupted view of surface temperature variability.

We collected cores from a 3-m coral colony (*Porites lutea*) from Beau Vallon Bay, Mahe Island (4°37′S, 55°49′E), using a sea-water-based hydraulic wire line drill. The coral was found growing at a depth of 7 m and was 300 m outside the reef front in an area with no terrestrial influence (*9*). We only analyzed the top 2.2 m of the core (*10*), because below this depth, changes in the coral's growth axis precluded a continuous record.

The complete coral oxygen isotope record is shown in Fig. 2 as a time series. Annual density bands are present in the coral and help to provide a chronometer for the isotopic record. The growth rate of the coral averages 14 mm per year, and our 1-mm sample spacing provides approximately monthly resolution. There is a strong seasonal cycle in $\delta^{18}O$, and, rather than relying completely on the sporadically weak density banding, we used the seasonal $\delta^{18}O$ cycle to count annual layers in the coral. We assigned the high $\delta^{18}O$ extremes to August 1 of every year (on average, the coldest time of the year) and interpolated linearly between these anchor points for all other age assignments. This approach undoubtedly creates the potential for a 1- to 2-month time-scale error in any given year, but it is the most objective method. We date the single largest coral $\delta^{18}O$ anomaly to late in 1877, which precisely matches the most catastrophic monsoon failure on record (Fig. 2A).

The coral $\delta^{18}O$ at this location is a relatively simple proxy for SST. In general, coral $\delta^{18}O$ depends not only on the temperature but also on the $\delta^{18}O$ of the ambient seawater. At the Seychelles, however, one would expect the seasonal temperature variability (of more than 2°C) to dominate the nearly constant $\delta^{18}O$ of seawater (*11*). A rigorous test of the proxy is that coral $\delta^{18}O$ anomalies (calculated by removal of the average seasonal cycle) correlate strongly with observed monthly SST anomalies over the last 15 years (Fig. 2B). Furthermore, correspondence with an independent index of monsoon strength (*4*) demonstrates that the coral successfully captures

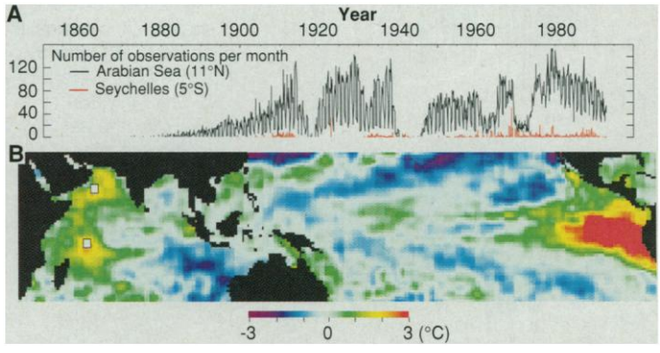

Fig. 1. (**A**) Time series of the number of instrumental observations per month (*26*) in the grid boxes including the Seychelles and the Arabian Sea [the locations are indicated in (B) by the white boxes]. The Arabian Sea is widely considered to be one of the best observed regions for SST, but significant data gaps occur during the war years (1917 to 1920 and 1940 to 1945) and before 1900. (**B**) July 1983 minus July 1984 SST anomalies, derived from the SST data in (*24*), illustrating the sensitivity of the western Indian Ocean to ENSO phase changes.

the large-scale aspects of Asian monsoon behavior (Fig. 2C).

The length and resolution of the coral record allow a detailed characterization of the Indian Ocean SST spectrum (Fig. 3). Over the full record, $\delta^{18}O$ values decreased by about 0.15 per mil, which, if entirely temperature-related, implies that SSTs warmed by 0.8°C. The structure of this long-term trend is identical to that in instrumental SST records (*8*), but the magnitude of inferred warming is substantially larger in the coral. The most prominent cyclical mode has a decadal periodicity (11.8 to 12.3 years) and is relatively constant in amplitude throughout the record. On interannual time scales, several frequencies are evident, namely from 5.0 to 5.5 years, from 3.5 to 4.0 years, and from 1.7 to 2.4 years (*12*). The amplitudes of these interannual modes varied substantially over the last 150 years (*13*). For example, the 3.5-year mode was strong before 1920 and after 1960 but weak between these times. Conversely, the amplitude of the 5-year mode was strongest in the 1930s and 1940s. The energy in the 1.7- to 2.4-year band was apparently modulated by the decadal cycle: the amplitude varied with the same characteristic period (roughly 12 years).

Comparison with other time series is one way to deduce the mechanisms for concentration of variance in these frequencies. For interannual variability in the coral record, broad regional connections are remarkably clear: virtually identical temporal patterns result from the analysis of Pacific coral and climate records that reflect the ENSO phenomenon. The coral $\delta^{18}O$ record from Tarawa Atoll (western Pacific) (*14*) captures a 100-year-long history of the eastward migrations of the Indonesian Low, and, therefore, correlation with the Seychelles record provides a test of zonal pressure gradient influences. An analogous (but inverse) test can be applied with the use of the Seychelles coral and Darwin sea level pressure records (*15*).

Filtering of the 3- to 6-year period in these records (Fig. 4) demonstrates that the zonal ENSO connection has persisted simply and directly for at least 100 years, despite the changing dominant frequencies of the ENSO phenomenon and without being confounded by processes unique to the Indian Ocean. Therefore, even though the relation between India monsoon rainfall and the ENSO indices is nonstationary (*16*), the relation between the tropical Indian Ocean SST and the ENSO has been essentially constant. Given that constancy, the Seychelles record clarifies and extends two aspects of the ENSO phenomenon: its tendency to cluster around either 3.5- or 5.3-year periods and the fact that the longer periodicity was favored during the most pronounced monotonic rise in average tropical ocean temperatures.

The strength of the ENSO correlations attests to the importance of zonal excursions of the Indonesian Low as a primary control on climate variability throughout the tropics, but the decadal cycles that actually dominate the Seychelles coral record must reflect a separate process. Decadal modes are common in long tropical Pacific climate records but are not as strongly expressed, and the frequency is not as consistent as in the Seychelles (*17*). Decadal filters (Fig. 4) show generally weak correlation between these cycles in the Pacific records and the relatively more energetic cycles in the Seychelles record. Therefore we cannot call upon a strictly tropical Pacific phenomenon to explain the lower frequency variability in the coral.

Instead, we suggest that the decadal mode in the Seychelles coral is characteristic of the Asian monsoon system. For example, decadal cycles in the India Monsoon Rainfall Index (*18*) correlate strongly with those in the coral over most of the period of record overlap (Fig. 4). In fact, the overall correlation between unfiltered Seychelles coral $\delta^{18}O$ anomalies and the India Monsoon Rainfall Index is uniformly high (r = 0.6) before the late 20th century. The sense of the relation is as expected from considerations of annual and biennial variability: negative $\delta^{18}O$ (warm SST) anomalies correspond with weak monsoons, and positive anomalies (cool SST) follow strong monsoons. In all the extreme cases (weak or strong monsoon), the SST anomalies lag the monsoon rainfall anomalies by 1 to 8

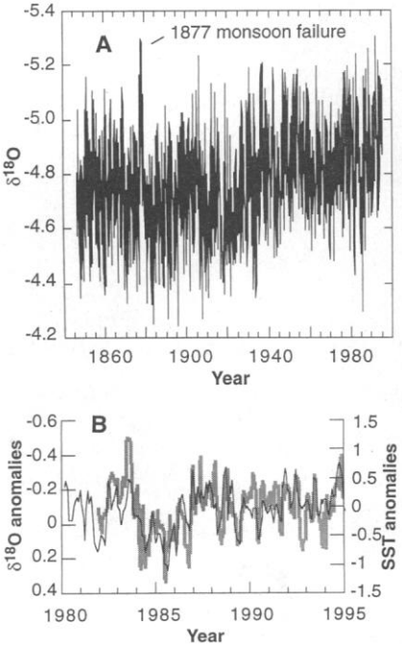

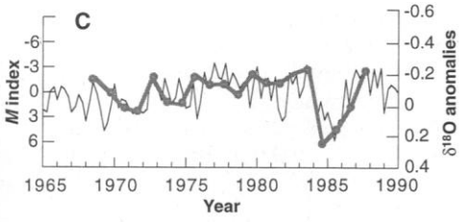

Fig. 2. (**A**) Complete coral $\delta^{18}O$ time series. The year 1877 contains the single largest seasonal anomaly. (**B**) Monthly coral $\delta^{18}O$ anomalies (deviations from average seasonal cycle) (thin line) follow monthly SST anomalies (thick gray line) [from (*24*)] over the last 16 years of data coverage (correlation coefficient r = 0.72). (**C**) Seasonal coral $\delta^{18}O$ anomalies (thin line) also correlate with the M index of Asian monsoon intensity (thick gray line) [from (*4*)] over the period 1968 to 1991.

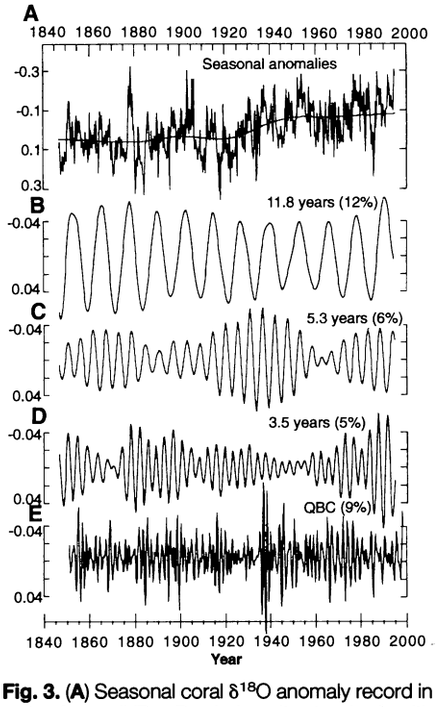

Fig. 3. (**A**) Seasonal coral $\delta^{18}O$ anomaly record in units of per mil (Pee Dee belemnite standard), with the long-term trend superimposed. (**B** through **E**) SSA decomposition of the Seychelles coral $\delta^{18}O$ anomalies in various frequency bands (*13*), with the approximate period and percentage variance (of detrended anomaly record) indicated for each significant mode. Each reconstruction shown is the sum of two modes in quadrature, except for the quasi-biennial mode (E), which sums a total of four modes (two sets in quadrature). QBC, quasi-biennial cycle.

months. Over decadal periods, there is no detectable phase difference between the two indices. The correlation breaks down in the late 20th century, but the coral follows large-scale monsoon indices during this interval (Fig. 2C), whereas the rainfall record does not (*4*).

Independent of these uncertainties in instrumental records of monsoon intensity, the coral record suggests that the same decadal-scale processes that are responsible for strong Seychelles SST variability also govern the strength of the quasi-biennial cycle, which is, undeniably, the dominant form of monsoon variability (*18*, *19*). Throughout the tropics, the quasi-biennial cycle has a geographic expression similar to that of the ENSO (*20*), and previous analyses of tropical SST compilations have demonstrated a decadal modulation of its amplitude (*21*). We show here (Fig. 4) that this amplitude modulation in Darwin sea level pressure correlates with the decadal mode in the Seychelles coral. Intervals of high quasi-biennial variability are associated with periods of warm SST at the Seychelles, corresponding to the weak monsoon phase of the quasi-biennial cycle (*19*).

There are several possible explanations for this decadal variability in records that have the Asian monsoon as a common influence. One is that Northern Hemisphere midlatitude circulation processes, perhaps even associated with North Pacific gyre variability (*22*), create snowfall anomalies that alter the strength of the monsoon and ultimately lead to SST changes (by affecting the intensity of wind-driven upwelling and evaporative cooling). Another is that processes in the southern Indian Ocean contribute decadal-scale variability to the equatorial system (*23*) and subsequently to the Asian monsoon through moisture and latent heat convergence. It is also possible that the biennial cycle could be rectified regionally to amplify any existing decadal periodicity. Although it will require a larger collection of long records to discriminate between these alternatives, it is apparent that all of these scenarios imply significant interaction between the tropics and midlatitudes, channeled through the monsoon system.

In summary, the coral record shows that the interannual variability in the western equatorial Indian Ocean has been related directly to that of the equatorial Pacific for over a century. This observation immediately simplifies modeling of the global ENSO phenomenon and any climate change associated with the redistribution of SST, for example, rainfall in East and South Africa. On the other hand, the propagation of decadal-scale variability through the monsoon, which was apparently an important process in the preanthropogenic climate of the Indian Ocean, is, in all likelihood, not such an immutable feature of the climate system (see Fig. 4). By preserving a long index (which is, in principle, capable of extension to many centuries) of both Asian monsoon and ENSO intensity at seasonal resolution, the coral provides a unique perspective on the interaction between these processes and their characteristic time scales. For example, if the quasi-biennial cycle is part of the ENSO phenomenon (*7*), its decadal amplitude modulation may represent the clearest example of monsoonal processes influencing interannual climate variability in the tropics, in this case implying an active, rather than passive, role of the Asian monsoon.

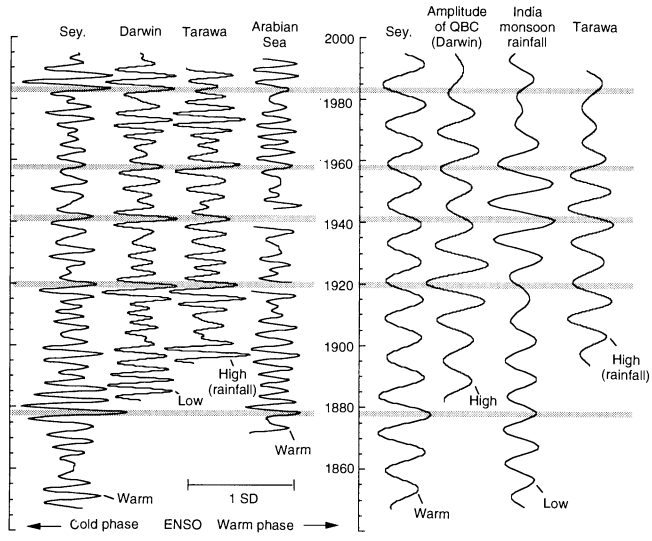

Fig. 4. Band-pass–filtered versions of various climate time series discussed in text. We took the Arabian Sea SST data from (*8*). The records were normalized to unit variance, and the scale (in units of standard deviation) is the same for all records. The left panel shows the ENSO band (3 to 6 years), and the right panel shows the decadal band (9 to 16 years). To estimate the decadal modulation of the tropical quasi-biennial cycle, we first rectified a version of Darwin sea level pressure filtered at 1.4 to 2.9 years and then subjected this rectified series to the decadal band pass. The filtered records are oriented so that the ENSO "warm phase" response is to the right, and the polarity is as indicated at the bottom of each record. Shaded bars highlight several strong El Niño years for general reference and for illustration of phase. Sey., Seychelles.

REFERENCES AND NOTES

1. Y. M. Tourre and W. B. White, *J. Phys. Oceanogr.* **25**, 1317 (1995).
2. G. Philander, *El Nino, La Nina and the Southern Oscillation* (Academic Press, San Diego, CA, 1990).
3. P. J. Webster *et al.*, *J. Geophys. Res.*, in press.
4. P. J. Webster and S. Yang, *Q. J. R. Meteorol. Soc.* **118**, 877 (1992).
5. T. P. Barnett, L. Dümenil, U. Schlese, E. Roeckner, *Science* **239**, 504 (1988).
6. S. Hastenrath, A. Nicklis, L. Greischar, *J. Geophys. Res.* **98**, 20219 (1993).
7. G. Meehl, *Mon. Weather Rev.* **115**, 27 (1989).
8. A local air temperature and rainfall record from Mahe island extends to 1894, but the station moved its location and elevation substantially several times throughout this period. Therefore, for the purposes of time series analysis, these records are highly discontinuous. The extent and quality of SST observations before 1980 from surrounding areas of the Indian Ocean are summarized by M. Bottomley *et al.* [*Global Ocean Surface Temperature Atlas "GOSTA"* (United Kingdom Meteorological Office, Bracknell, UK, 1990)].
9. G. Faure, "Project Report: Research into the origin of the degradations of the recifal populations of Beau-valon Bay Mahe Island Republic of Seychelles" (Seychelles Public Utilities Commission, Victoria, Seychelles, 1989).
10. We slabbed and x-rayed the 1-inch-diameter coral cores and then took 0.1- to 0.5-mg carbonate powder samples along an axis of constant growth, using a variable speed drill with a 1-mm bit. In general, the sampling was normal to the growth axis, but over a few specific growth bands, irregular growth affected the sampling. These bands were analyzed in duplicate or triplicate along different axes to ensure an unbiased record. For isotopic analysis, we used an automatic carbonate preparation device (optimized for efficient throughput of samples) attached to a Finnegan MAT252 gas source mass spectrometer at the Scripps Institution of Oceanography. Long-term reproducibility in this fast method, deduced from 350 determinations of a carbonate standard analyzed along with the coral samples, is less than 0.08 per ml for $\delta^{18}O$. The value of $\delta^{18}O$ is

$$\delta^{18}O = \left[\frac{(^{18}O/^{16}O)_{sam}}{(^{18}O/^{16}O)_{std}} - 1\right] \times 1000$$

where sam is sample and std is the Pee Dee belemnite reference standard.
11. Gridded SST values (*24*) show a seasonal cycle of nearly 3°C for the grid box including Mahe. Recent calibrations of Porites $\delta^{18}O$ variability (*25*) suggest a temperature dependence of about 0.18 per mil/°C; when this scaling is used, our coral seasonality predicts a seasonal temperature change of about 2.5°C. For comparison, the air temperature record from Mahe (courtesy of the Seychelles Meteorological Department) suggests a surface temperature seasonality of only 2°C. These apparent discrepancies of several tenths of a degree Celsius between the magnitude of seasonal cycles in coarse-gridded SST observations and the coral $\delta^{18}O$ cycle are probably the result of the inherently different sampling approaches and, in any case, do not affect considerations of interannual variability. Although seawater $\delta^{18}O$ has not been monitored continuously, simple scaling of the 0.4 per mil seasonal salinity variability by means of standard tropical $\delta^{18}O$-salinity relations results in less than 0.1 per mil seasonal $\delta^{18}O$ seawater change. Unpublished, handwritten records, courtesy of the Seychelles Meteorological Department, show a strong semiannual rainfall signal that does not measurably affect the coral $\delta^{18}O$ seasonal cycle; the interannual variability in the local rainfall seldom exceeds 50% and is too weak to produce a measurable isotopic effect. Thus, we conclude that the hydrological cycle does not complicate substantially the temperature interpretation of the $\delta^{18}O$ record.
12. The exact frequency of peak variance depends on the spectral technique used. Applying Blackman-

Tukey methods [G. M. Jenkins and D. G. Watts, *Spectral Analysis and its Applications* (Holden-Day, Oakland, CA, 1968)] to the $\delta^{18}O$ anomalies resolves statistically significant (minimum of 80% level) spectral peaks at 12.2-, 8.3-, 5.5-, 3.78-, 2.3-, and 1.7-year periods. The maximum entropy method places these peaks at 11.4, 7.8, 5.5, and 3.5, 2.3, and 1.7 years.

13. We used singular spectrum analysis (SSA) [R. Vautard and M. Ghil, *Physica D* **35**, 395 (1989)] to reconstruct the most energetic modes in the coral record. After the removal of the seasonal cycle and the long-term trend, with a window length of M = 39 years, SSA produces two modes in clean quadrature: modes 1 and 2, with a period of 11.8 years, and modes 3 and 4, with a period of 5.3 years (modes with periods greater than 39 years are unresolved). After the further removal of the decadal and interdecadal modes and with a window length of M = 25 years, two modes emerge in quadrature: modes 1 and 2, with a period of 5.3 years, and modes 3 and 4, with a period of 3.5 years. The quasi-biennial signal emerges in clean quadrature when a 10-year window length is used. Monte Carlo simulations suggest that all of these modes represent statistically significant (at the 95% confidence level) concentrations of variance. More conventional band-pass filtering yields nearly identical patterns.
14. J. E. Cole *et al.*, *Science* **260**, 1790 (1993).
15. Darwin sea level pressure anomalies were supplied to us by R. Allan of the Commonwealth Scientific and Industrial Research Organization. Pressure anomalies at Darwin lead the Seychelles coral anomalies by 3 to 5 months throughout most of the period of record overlap. However, the zero phase correlation across the entire 3- to 6-year band is 0.79, and cross-spectral estimates suggest that over 80% of the variance in the 3.5- and 5.3-year periods is coherent.
16. A. J. Troup, *Q. J. R. Meteorol. Soc.* **91**, 490 (1965).
17. R. B. Dunbar *et al.*, *Paleoceanography* **9**, 291 (1994).
18. B. Parthasarthy, K. R. Kumar, A. A. Munot, *Proc. Indian Acad. Sci. Earth Planet. Sci.* **102**, 121 (1993).
19. G. A. Meehl, *Science* **266**, 263 (1994).
20. T. P. Barnett, *J. Clim.* **4**, 269 (1991).
21. ———*Geophys. Res. Lett.* **16**, 803 (1989).
22. M. Latif and T. P. Barnett, *Science* **266**, 634 (1994).
23. R. J. Allan *et al.*, *J. Clim.* **8**, 1853 (1995).
24. R. W. Reynolds and T. M. Smith, *J. Clim.* **7**, 929 (1994).
25. M. Gagan, A. R. Chivas, P. J. Isdale, *Earth Planet. Sci. Lett.* **121**, 549 (1994).
26. R. J. Slutz *et al.*, comprehensive Ocean-Atmosphere Data Set, Release 1 (Climate Research Program, Boulder, CO, 1985).

27. We thank J. Ardai, K. Broad, and A. Hilton for technical support; D. Laredo from the Seychelles Public Utilities Commission and S. Marshall of the Seychelles Ministry of Foreign Affairs, Planning and Environment for facilitating the field work; and M. Moore and D. Schrag and other reviewers for useful discussion. D.E.H. was supported through a Department of Energy–Oak Ridge Institute for Science and Education graduate fellowship. The project itself was sponsored by the National Oceanic and Atmospheric Administration Scripps-Lamont Consortium.

31 January 1997; accepted 30 June 1997

Realization of a Functional Cell for Quantum-Dot Cellular Automata

A. O. Orlov, I. Amlani, G. H. Bernstein, C. S. Lent, G. L. Snider

This paper presents an experimental demonstration of a basic cell of the quantum-dot cellular automata, a transistorless approach to computation that addresses the issues of device density, interconnection, and power dissipation. The device under study was composed of four metal dots, connected with tunnel junctions and capacitors, and operated at <50 mK. Operation was evidenced by switching of a single electron between output dots controlled by a single electron switching in input dots, demonstrating a nonlinear, bistable response.

Achievement of ever higher levels of integration in microelectronics eventually will require a shift from the field-effect transistor (FET)–based paradigm. Scaling of FETs will be limited by unacceptable power dissipation and short-channel effects, which lead to performance degradation. One alternative architecture, quantum-dot cellular automata (QCA) (*1*), is a transistorless approach with quantum dots that addresses the issues of device density, interconnection, and power dissipation. Conventional digital architectures use transistors as current switches to charge and discharge capacitors to the required logic voltage levels. In QCA, logic states are encoded no longer as voltages but rather by the positions of individual electrons. QCA architecture is scalable to molecular levels, and performance actually improves as the size of the device is decreased. The cell presented here operates at cryogenic temperatures, but a molecular-sized QCA cell would function at room temperature.

On the basis of existing technology, a possible realization of a basic QCA cell would be composed of two series-connected metal dots separated by tunneling barriers and capacitively coupled to a second, identical double dot. The dots and associated capacitances are sufficiently small that the system is in the Coulomb blockade regime (*2*) at the temperature of the experiment. If the cell is biased so that there are two excess electrons within the four dots (one excess electron per double dot), those electrons are forced to opposite corners of the four-dot system by Coulomb repulsion. The two possible polarization states of the system represent logic 0 and 1, as indicated in Fig. 1A. Properly arranged, arrays of these basic cells can implement Boolean logic functions (*3*).

We report the experimental demonstration of a functioning QCA cell. Direct measurements of the charging diagram of output dots under the influence of electron switching in input dots, combined with electrometer measurements of output dots, show a controlled polarization change of a QCA cell. Our experimental results show excellent agreement with theory.

The device consists of four Al islands, with input dots D1 and D2 and output dots D3 and D4 (Fig. 1B). The Al-AlO_x-Al tunnel junctions were fabricated on an oxidized Si substrate by a standard electron beam–lithography and shadow evaporation technique (*4*). The area of the junctions is about 60 by 60 nm. The sample was mounted on the cold finger of a dilution refrigerator with a base temperature of 15 mK. Conductances of the double dot and each input dot were measured simultaneously by standard ac lock-in techniques with an excitation voltage of 4 μV at 16 to 40 Hz. A magnetic field of 1 T was applied to suppress the superconductivity of the metal. Typical resistance of a single junction at 1 K was 200 kilohm. Capacitances between gates and islands were determined from the period of the Coulomb blockade oscillations, and values of junction capacitances were extracted from current-voltage measurements (*2*).

A polarization change of the QCA cell requires an electron transfer between dots within each double dot. Gate electrodes force an electron to switch from one dot to the other within the input set of dots, which in turn induces a switch of the other electron in the output dots. This process can best be understood by considering the motion of electrons within one double dot. By measuring the conductance through the double dot as a function of the gate voltages V_C and V_D (Fig. 1C), we can determine the electron charge configuration within the double dot. Current can flow through a double dot only at certain settings of the gate voltages, where the Coulomb blockade is lifted for both dots simultaneously. A contour plot of the measured conductance through a double dot as a function of gate voltages V_C and V_D (Fig. 1D) shows peaks in conductance at triple points, T, which form a hexagonal "honeycomb" (*5*). Each hexagonal cell is delineated by dashed lines in Fig. 1D,

Department of Electrical Engineering, University of Notre Dame, Notre Dame, IN 46556, USA.